Toward the Controlled Synthesis of Hexagonal Boron Nitride Films

Ariel Ismach,[†,*] Harry Chou,[†] Domingo A. Ferrer,[‡] Yaping Wu,[§] Stephen McDonnell,[⊥] Herman C. Floresca,[⊥] Alan Covacevich,[†] Cody Pope,[†] Richard Piner,[†] Moon J. Kim,[⊥] Robert M. Wallace,[⊥] Luigi Colombo,[∥] and Rodney S. Ruoff[†]

[†]Department of Mechanical Engineering and the Materials Science and Engineering Program and [‡]Department of Electrical Engineering and Computer Engineering, The University of Texas at Austin, Austin, Texas 78712, United States, [§]Department of Physics, Xiamen University, Xiamen 361005, People's Republic of China, [⊥]Department of Materials Science and Engineering, The University of Texas at Dallas, Dallas, Texas 75080, United States, and [∥]Texas Instruments, 13121 TI Boulevard, Dallas, Texas 75243, United States

ABSTRACT

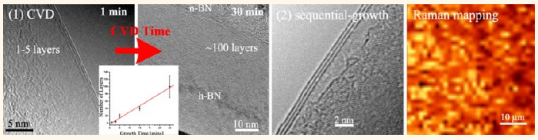

Atomically smooth hexagonal boron nitride (h-BN) layers have very useful properties and thus potential applications for protective coatings, deep ultraviolet (DUV) emitters, and as a dielectric for nanoelectronics devices. In this paper, we report on the growth of h-BN by a low-pressure chemical vapor deposition (LPCVD) process using diborane and ammonia as the gas precursors. The use of LPCVD allows synthesis of h-BN with a controlled number of layers defined by the growth conditions, temperature, time, and gas partial pressure. Furthermore, few-layer h-BN was also grown by a sequential growth method, and insights into the growth mechanism are described, thus forming the basis of future growth of h-BN by atomic layer epitaxy.

KEYWORDS: hexagonal boron nitride · h-BN · CVD · sequential growth · 2D Raman mapping

Layered materials have attracted scientific and technological interest due to their highly anisotropic properties.[1] This interest has increased since the controlled exfoliation[2,3] and synthesis[4] of single- and few-layer graphene was demonstrated. The mechanical exfoliation technique has been successfully applied to a wide range of layered compounds.[5] However, in contrast to graphene, there have been only a few synthetic approaches to achieve large-area single- or few-layer films of other layered materials. Recently, another layered material that has attracted significant interest is hexagonal boron nitride (h-BN), sometimes referred as "white graphite/graphene" due to its structural similarity with graphite and large band gap. The boron and nitrogen atoms are arranged in a hexagonal lattice with a lattice parameter of 0.25 nm, in comparison to graphene's 0.249 nm, with the BN layers stacked in the AA′ configuration. The interest in the synthesis of thin BN films and coatings with controlled structure is due to their mechanical, thermal, and chemical properties. Up until recently, BN has been used mainly as a high-temperature ceramic.[6,7] Obtaining either h-BN or cubic (c-BN) has proven to be very challenging, and a mixture of cubic, hexagonal, "nanocrystalline" (also referred to as turbostratic, t-BN), and amorphous BN was typically obtained.[6,7] It was only in 2004 that Kubota *et al.*[8] showed the recrystallization of h-BN powder into high-quality microcrystals at high temperatures and its use for deep UV optoelectronic devices.[9] The synthesis of single- or few-layer h-BN was first obtained in ultrahigh vacuum systems, mostly using borazine as the precursor and single-crystal transition metals as the substrates.[10−13] These early attempts were followed by recent reports using atmospheric pressure (APCVD)[14] and low-pressure chemical vapor deposition (LPCVD),[15−19] driven mainly by the potential application of monolayer or few-layer h-BN as a dielectric material for graphene-based electronic devices.[20,21] However, a facile and rational method to synthesize high-quality h-BN films with a controllable number of layers is needed in order to fulfill the entire spectrum of h-BN potential applications, such as mechanical and thermal coatings, DUV optoelectronic devices, and for nanoelectronic devices, as well as for fundamental studies of the basic properties of this material.

Here, we report on the controlled synthesis of h-BN from ammonia and diborane, precursors commonly used in the microelectronics industry, in an LPCVD growth system.

* Address correspondence to aismach@austin.utexas.edu.

Received for review May 2, 2012 and accepted June 17, 2012.

Published online June 18, 2012
10.1021/nn301940k

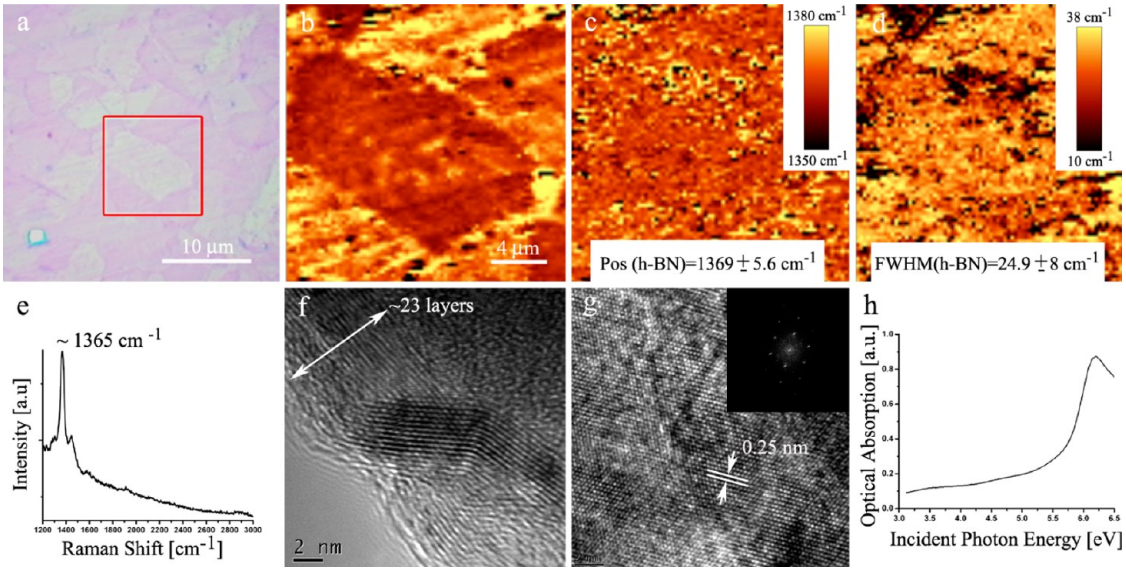

Figure 1. h-BN film characterization. (a) Optical image. (b) Scanning Raman mapping with the h-BN signal at ~1365 cm^{-1} of the red square region indicated in (a). (c,d) Mapping of the position and fwhm of the h-BN peak, respectively. (e) Raman spectra at the center of (b) with a 45 s integration time. (f,g) TEM characterization showing the layered structure and the hexagonal lattice, respectively. The inset shows an FFT of the image in (g). (h) UV−vis absorption spectra of an h-BN film, with ~40 layers, transferred to a fused silica substrate after removing the background from the substrate.

The growth of h-BN films with a different number of layers was successfully achieved by tailoring the CVD growth parameters. In addition, we also describe the synthesis of few-layer h-BN films by a sequential growth method (similar to atomic layer deposition/epitaxy). The h-BN films were characterized by transmission electron microscopy (TEM), Raman spectroscopy, 2D Raman mapping, X-ray photoelectron spectroscopy (XPS), scanning probe microscopy (SPM), UV−visible spectroscopy, and optical microscopy. The possible mechanisms of growth are also described and discussed.

RESULTS AND DISCUSSION

In order to establish the structure of the BN films, we performed TEM, selected area electron diffraction (SAED), and Raman spectroscopy. Boron nitride has a Raman signal at ~1365 cm^{-1} which arises from the E_{2g} phonon and is characteristic of the h-BN phase.[22] A nanocrystalline phase (a disordered h-BN phase, sometimes referred to in the literature as turbostratic, t-BN) would also generate this h-BN Raman signal, due to the hexagonal arrangement of the BN lattice, but not necessarily due to the BN having a *planar* layered structure (see Figure SI1 in the Supporting Information). Therefore, in order to ensure that the BN is hexagonal with a *planar* layered structure, we characterized all of the samples in this article by Raman spectroscopy, 2D Raman mapping, TEM, SAED, and in many cases also XPS and UV−visible spectroscopy. Figure 1 shows a set of data from a typical BN film grown on a Ni foil at 1025 °C for 5 min with a B_2H_6/NH_3 ratio of 1/18 at a pressure of about 135 mTorr. Figure 1a shows an optical microscope image of a large-area few-layer h-BN sample after its transfer onto a 300 nm thermally grown SiO_2 film on a Si substrate. A Raman map of the h-BN signal at ~1365 cm^{-1},[22] shown as the red square area in panel a, is shown in Figure 1b. There is a clear h-BN peak intensity difference in the center of the image, and this we associate with different growth processes on different Ni grains. Figure 1c shows the Raman map of the spectral position of the h-BN peak, and Figure 1d shows the Raman map of the full width at half-maximum (fwhm) of the same area in Figure 1b. No significant differences appear in these maps, suggesting that the different intensities of the BN peak arise from variation in the number of layers across the film. Further studies of the influence of the Ni grain orientation on the growth characteristics are underway. The full Raman spectrum of the BN film with a 45 s integration time is also shown in Figure 1e. A plane-view TEM image of a ~23 layer film is shown in Figure 1f, in which the layered structure is imaged along crack edges in the film. The BN lattice shown in Figure 1g by HRTEM shows a hexagonal pattern with a 0.25 ± 0.01 nm lattice parameter, indicating that the BN structure has a layered hexagonal structure; the FFT of the TEM image is also shown in the inset displaying hexagonal symmetry. Growth was also performed on other substrates such as sapphire and copper foils, the latter commonly used as the substrate for graphene[4] and h-BN;[16−19] however, in all of our attempts on the growth of BN on Cu, a nanocrystalline BN (n-BN, *i.e.*, t-BN) was obtained (see Figure SI1).

UV−visible spectra were also taken to reconfirm the presence of h-BN as well as to determine the band gap of the film. In Figure 1h, the optical absorption of the film is plotted as a function of the incident wavelength from

which the band gap was extracted. The optical band gap was extracted by using the relationship used for direct band gap semiconductors: $\alpha = [A(E - E_g)^{1/2}/E]$,[23,24] where α is the absorption coefficient, E_g is the optical band gap energy, E is the incident photon energy, and A is a proportionality constant. On the basis of these data, an E_g of 5.75 eV was calculated (see Supporting Informaiton for details).

The growth of h-BN on single-crystal transition metals in UHV systems was reported to be surface-limited, and thus after a full monolayer was formed, the growth rate significantly decreased or completely stopped.[10−13] However, it was also reported that a monolayer grown in UHV conditions using diborane and ammonia precursors on Ni(100) could be used as a substrate for further growth in a metal−organic CVD reactor using ammonia and triethylboride as the precursors.[25] Although the growth of multilayer (films of 5−50 nm) h-BN on Ni surfaces was reported,[14] no detailed characterization and clear description were given. In the work described here, the average thickness (number of layers) of the h-BN films was found to have a linear dependence on the growth time (Figure 2e), as extracted from the TEM images in Figure 2a−d of samples grown at different growth times: 1, 5, 15, and 30 min. XPS data also suggest the increase in thickness with the growth time (discussed below). The analysis of the Raman maps with the h-BN peak at ~1365 cm^{-1} shows that there is no correlation of the peak position and full width at half-maximum (fwhm) with the number of layers (see Figure SI3). The influence of the growth temperature was also studied, and at lower temperatures (<800 °C), nanocrystalline BN (n-BN) is mainly obtained (see Figure SI4).

One conclusion from our experimental results is that the growth is not surface-limited as is often observed and reported for graphene on Cu.[4,26,27] On the other hand, the segregation and precipitation of B and N to form h-BN, as occurs for the growth of multilayered graphene or graphite on sufficiently thick Ni substrates,[26] is not likely to be the case either. This is so because the solubility of boron and nitrogen in nickel is very low at 1025 °C.[28,29] However, ammonia can be catalytically decomposed at nickel surfaces,[30] and a metastable Ni_3N phase could be formed at the surface.[31] This phase was found to be stable up to ~405 °C,[32] suggesting its decomposition prior to the h-BN formation. Diborane thermally decomposes at the CVD temperatures studied in this paper, 800−1000 °C. Its fate in the presence of ammonia involves a series of reactions involving its decomposition into boranes and their reaction with ammonia to form borazine that upon dehydrogenation forms BN.[33] Furthermore, boron was also found to react with Ni to form a metastable nickel boride phase.[34] After ruling out surface-limited growth and segregation and precipitation from the bulk (such as typically occurs for the growth of graphene on Ni), we considered reactions in the gas phase and solid−gas reactions involving Ni−B and Ni−N phases, as discussed further below.

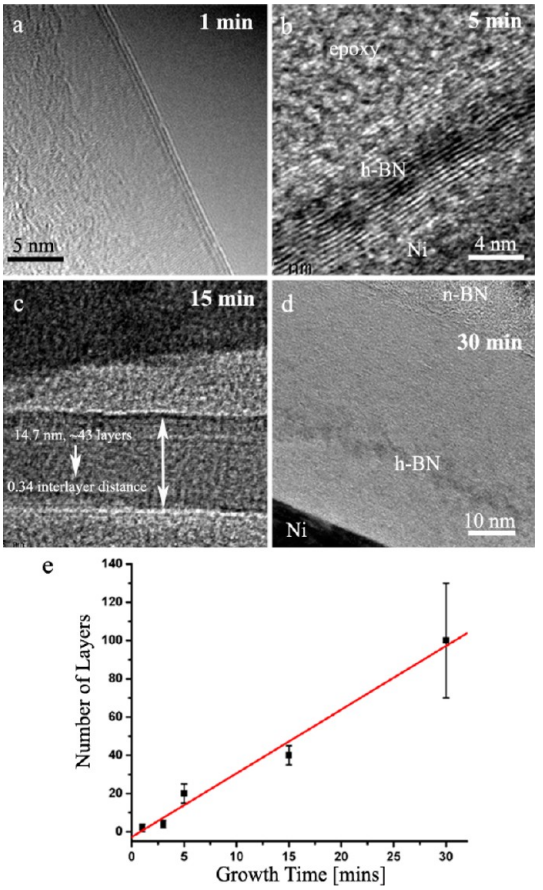

Figure 2. Number of layers as a function of growth time. (a−d) TEM images for samples grown for 1, 5, 15, and 30 min, respectively. (e) Average number of layers as measured in the TEM as a function of growth time. The data are shown as black dots and the linear fit in red.

Gas phase nucleation and growth is another mechanism to consider; however, one would expect to have either a weak or no surface dependence on the growth of h-BN films. To study this possibility, BN films were grown on different substrates (details will be provided in a separate paper). Figure 3a shows a cross section HRTEM image of BN/sapphire grown under the same conditions as those grown on Ni shown in Figure 1d, that is, at 1025 °C for 30 min. The HRTEM image reveals that the films are different, in particular, the number of layers and the structure. The BN films on Ni (Figure 2d) exhibit an ordered layered structure of about 100 layers with a nanocrystalline termination (n-BN), while on the growth rate on sapphire is much lower, with only a few layers appearing to be partially ordered and the rest of the film n-BN. The thickness of the films on the different substrates was found to be 40−50 nm on Ni and about 15 nm on sapphire, including the nanocrystalline layer in both cases. However, the nanocrystalline BN termination was not observed on h-BN films grown on Ni for shorter times.

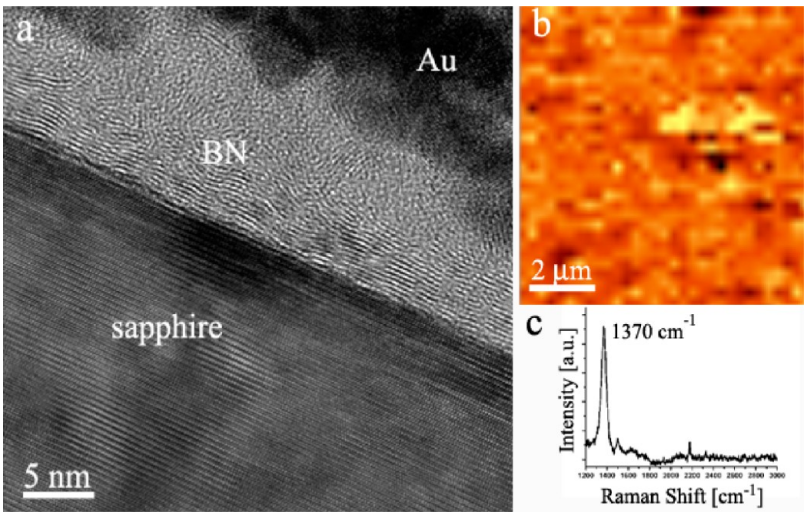

Figure 3. h-BN films on sapphire. (a) Cross section TEM of an h-BN film on sapphire. (b) Scanning Raman mapping, with (c) the h-BN peak and the Raman spectra.

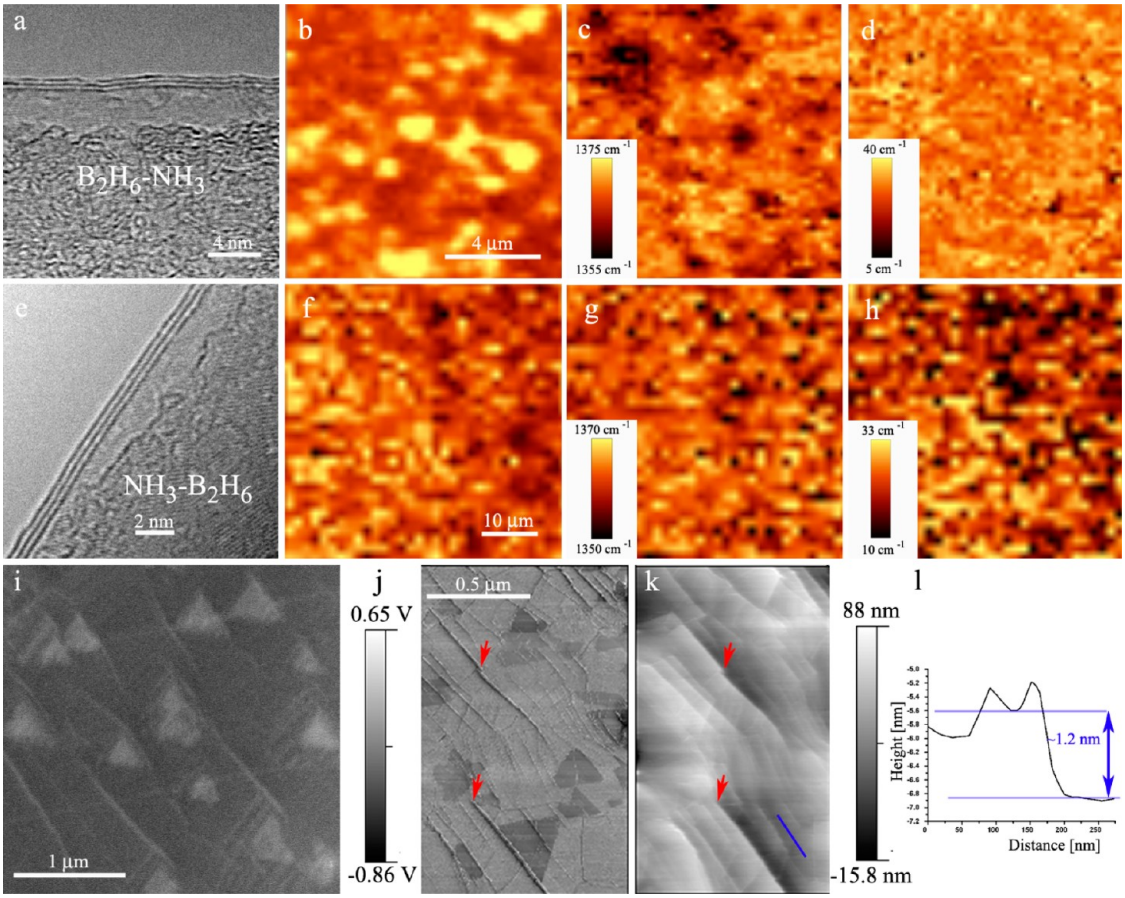

Figure 4. Sequential growth of h-BN films. TEM image, scanning Raman mapping with the h-BN peak intensity, position and fwhm, respectively: (a–d) for diborane-then-ammonia and (e–h) for ammonia-then-diborane. (i) SEM image showing triangular ad-layers and (j,k) LFM and topographic images of the same area. The triangular ad-layers are easily seen in the LFM image. The topographic image reveals the faceted Ni surface, and some ad-layers are also observable. The red arrows show reference points in both images, and the cross section along the blue line in (k) is shown in (l), with an ad-layer of ~1.2 nm height.

We suspect that the n-BN could arise from desorption from the reactor tube walls after the relatively long CVD process (>30 min) and redeposition on the sample substrate. The Raman characterization of a typical BN/sapphire sample is shown in Figure 3b,c and Figure SI5. Given the large observed differences between the

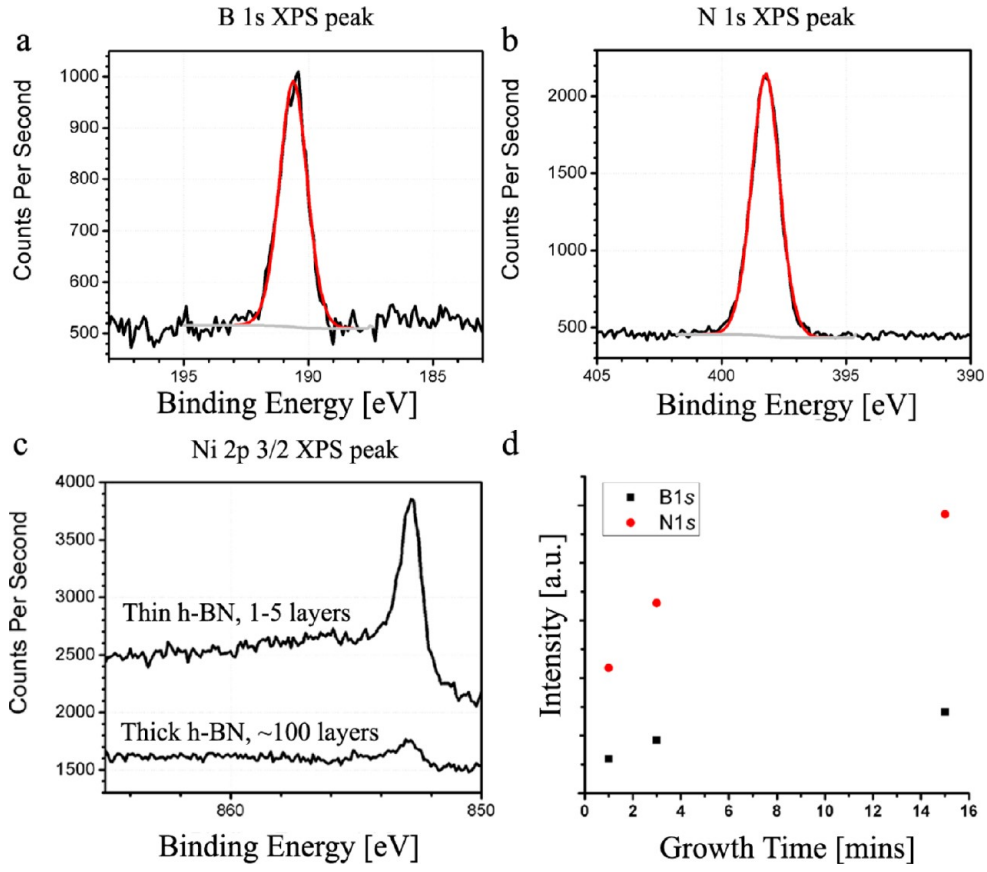

Figure 5. XPS characterization. (a) B1s and (b) N1s XPS peaks for the B−N bonding state, at 191.1 and 398.6 eV, respectively, in a thick h-BN film. (c) Analysis of Ni2p$_{3/2}$ peak for two samples with a different number of layers. The peak is more pronounced in the thinner h-BN film, corroborating the difference in the thickness between the samples and the absence of Ni in the h-BN film. (d) Intensities of the B1s and N1s peaks as a function of the CVD growth time. A clear increase in the B and N deposition is detected for samples with growth times of 1, 3, and 15 min.

h-BN grown on Ni and sapphire under the same conditions, we conclude that the growth of h-BN on Ni is not dominated by gas phase reactions.

Another possibility could be that the precursor gases decompose at the substrate surface and B and N stick to the surface followed by surface diffusion and reaction to form h-BN. This implies a sticking of atomic and/or molecular B or N species on the already formed h-BN layers that promote the formation of the multilayer structure with the observed dependence of the number of layers on the growth time.

In order to achieve a better understanding of the growth process, a sequential growth method was employed in which, similar to atomic layer deposition (ALD), the substrate surface is exposed to one of the precursors first for a given time (5 min), followed by a hydrogen flush for 10 min to ensure that any precursor residue is removed, and finally exposing the substrate to the ammonia for the same time (5 min). We found that the order of the precursor dosing does not play a significant role in the final average number of layers (measured by TEM), as shown in Figure 4, with 1−5 layers for *diborane-first* (Figure 4a) and 2−4 layers for *ammonia-first* (Figure 4e). The detailed Raman mapping and spectroscopy are shown in Figure 4b−d for the *diborane-then-ammonia* sample and Figure 4f−h for the *ammonia-then-diborane* sample, showing the intensity, position, and fwhm maps of the h-BN peak, respectively. In some areas of these samples, faceted (mainly triangular) ad-layers were observed. Figure 4i−kshows SEM, lateral force microscopy (LFM), and topographic images of such structures. The triangular shape may be formed by N-terminated edges, which have a lower calculated edge energy than B-terminated edges.[35−37] The topographic imaging (Figure 4k) of the same area in Figure 4jk shows the Ni facets while some h-BN ad-layers are barely visible due to the surface reconstruction of the Ni surface during the CVD growth process.

The sequential growth method might enable a better control over the surface chemistry during growth, limiting the reaction to the surface and inhibiting possible gas phase nucleation processes that might occur in a typical CVD-like procedure. The latter may reduce the film quality by the formation of 3D particles and by reducing the domain size. Furthermore, the sequential growth methodology would allow the grow of h-BN on nonregular/patterned surfaces and 3D

structures, thus enabling the assembly of more complex nanostructures and films, similar to the case of ALD.[38]

A detailed analysis of the XPS data on a variety of samples synthesized by both methods described above, that is, CVD (sample is exposed to both precursors *simultaneously*) and sequential growth (sample is exposed *sequentially* to each of the precursors), reaffirms the presence of the BN phase. Figure 5a,b shows the B1s and N1s XPS peaks, respectively, of a CVD-derived thick h-BN film shown in Figure 2d. The calculated atomic content was 42.48 and 42.04 at % for B and N, respectively. Carbon, oxygen, and nickel were also detected with 11.08, 3.73, and 0.67 at %, respectively. X-ray photoelectron spectroscopy results of all of the samples were very similar, leading to a B/N ratio of 1:1 with an error of about 0.05 at %. Thus, there is no measurable difference in the B/N ratio for samples with different number of layers and/or different method of synthesis. The Ni2p$_{3/2}$ peak appears to be stronger in thin films (1−5 layers, grown by the sequential growth method) than for the thick samples, as expected, corroborating the difference in thickness and the absence of Ni contamination in the h-BN film (Figure 5c). Additional indication for the thickness increase with the growth time can be seen in Figure 5d, where the intensities of the B1s and N1s XPS peaks are plotted as a function of the growth time for samples with growth times of 1, 3, and 15 min. A clear increase in the signal strength is detected up to 15 min growth (up to 40 ± 5 layers, 13.6 ± 1.7 nm, from TEM measurements), suggesting the increasing in B and N deposition. A sampling depth of ∼7 nm was calculated[39] for the B1s and N1s peaks, thus the signal is expected to reach its maximum around this value. Other parameters such as roughness on both the Ni and h-BN and film coverage could impact the measurement as well and are currently under study.

While the number of h-BN layers was not apparently affected by the order of the gas exposure, we found that the Ni/h-BN interface chemistry does change with the order of precursors in experiments using the sequential growth method. Figure 6 shows the B1s peak obtained from several samples. The XPS analysis shows the presence of B−Ni and B−O bonds for the films grown using the sequential process with *diborane-first* (Figure 6a). However, no trace of N, Ni−N, B−O, and B−Ni was found on the *ammonia-first* sample (Figure 6b). Control experiments in which the Ni foil was exposed to only one precursor at the CVD temperature (1025 °C) were performed and the surfaces analyzed by XPS. Ni−B and B−O bonds are readily detected in the sample exposed only to diborane at the CVD growth temperature (Figure 6c). However, in a similar experiment with ammonia only, no B−N, N, or Ni−N bonds were detected. These results suggest that the h-BN nucleation on Ni is dependent on dosing

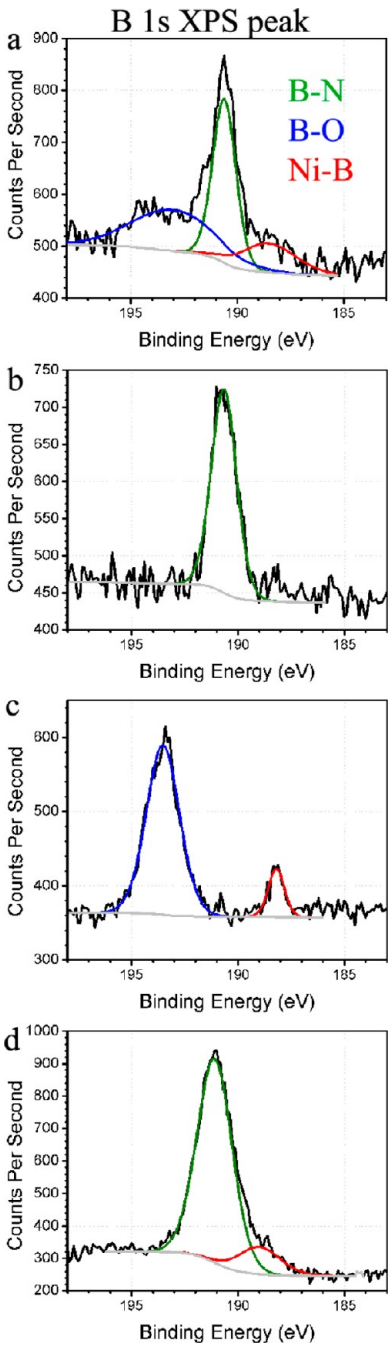

Figure 6. B1s XPS peak comparison. (a) Sequential growth with diborane first showing the peak deconvolution into B−N (190.584 eV), B−O (193.754 eV), and Ni−B states (188.79 eV). (b) Sequential growth with ammonia first exhibiting only the B−N bonding state (190.65 eV). (c) Ni−B (188.3 eV) and B−O (193.44 eV) peaks in a control experiment in which the Ni foil was exposed to diborane, and (d) thick h-BN film (∼100 layers) after sputtering with Ar-ion, showing the presence of B−N (191.09 eV) and Ni−B (188.98 eV) bonds. See Table SI1 for more details.

order, that is, diborane first or second. Ni−B bonds were also detected by XPS on CVD-grown h-BN after Ar-ion sputtering for a few seconds (Figure 6d), which suggests that the growth mechanism might be similar to the sequential growth in which the diborane is dosed first. However, it must be noted that Ar-ion sputtering

may cause a sample perturbation, and further careful experiments are needed to corroborate the presence of the Ni–B bonds in the CVD-grown samples. The difference in the binding energy (less than 1 eV) for the Ni–B and B–O bonds in the samples shown in Figure 6 could arise from phases with different stoichiometry. A possible explanation for the growth of h-BN by these two methods (CVD and sequential growth with diborane dosed first) is that the diborane decomposes and the boron reacts with the Ni to form a Ni–B phase which then further reacts with ammonia, leading to the formation of h-BN. Further studies are underway to elucidate the mechanisms associated with ammonia-first dosing.

CONCLUSION

We have shown a facile synthesis of h-BN with controllable thickness (number of layers) by both LPCVD and separately by a sequential growth method (sequential dosing of precursors), using gas precursors widely used in industry, diborane and ammonia. The use of gas precursors may have significant advantage over solid or liquid precursors in an industrial environment.[40] Characterization by Raman spectroscopy and 2D Raman mapping, TEM, XPS, and UV–vis was described. Despite lacking a complete understanding of the growth mechanism, nucleation by the reaction of Ni and B seems to be crucial in the growth by CVD from the gas mixture and by sequential dosing with diborane first and then ammonia. We also have shown that growth of h-BN on sapphire appears to be very different than for the growth of h-BN on Ni. The detailed surface chemistry of Ni–B–N as well as the influence of the nickel crystal orientation on the nucleation and growth of h-BN needs to be clarified in order to achieve better control of the h-BN film structure.

EXPERIMENTAL SECTION

A LPCVD chamber having a 25 mm diameter quartz tube with diborane, ammonia, and hydrogen as CVD precursors was used to grow h-BN films at various temperatures, gas pressure, and flow rates on Ni (50 μm thick, 99.5%, McMaster), Cu (25 μm thick, 99.8%, Alfa Aesar), and sapphire substrates (C-plane, McMaster). In a typical growth run, the substrate was placed in the quartz tube and pumped down to the base pressure of ~10 mTorr. Then hydrogen gas was introduced at a flow rate of 10 sccm H_2 (ultrahigh purity grade, Airgas), and the sample was heated to the desired temperature; once the target temperature was reached, ammonia (99.999%, Specialty Gases, Inc.) at flow rate of 18 sccm and diborane (5% in H_2, Matheson Tri-Gas) at 1 sccm were introduced into the system and the growth carried out for a preselected period of time. At the end of the growth run, all of the gases were turned off and the sample was cooled under Ar (~20 sccm, ultrahigh purity grade, Airgas) to room temperature. The BN films were first characterized directly on the Ni substrates; thereafter, the BN films were transferred to other substrates by chemically removing the Ni substrate by a method similar to those previously reported,[4,14] where the h-BN/Ni samples were coated with a thin layer of polymethylacrylate (PMMA, Sigma Aldrich) and then immersed in an iron chloride solution (0.5 M, 99.99%, Sigma-Aldrich) for ~3 h to completely etch the Ni away. The PMMA/h-BN films were then transferred to the target substrate, and the PMMA was dissolved in acetone, leaving the BN film. The samples were then characterized by Raman spectroscopy, 2D Raman mapping (Witec Alpha 300 micro-Raman confocal microscope), transmission electron microscopy (TEM, TECNAI TF20), selected area electron diffraction (SAED), scanning electron microscopy (SEM, FEI Quanta-600), optical microscopy (Zeiss Axiovert 100A Light Microscope), UV–visible spectroscopy (Cary 5000 UV–vis NIR spectrometer), and X-ray photoelectron spectroscopy (XPS, described in detail below).

A dual column scanning electron microscope/focused ion beam (SEM/FIB) system was used to prepare TEM samples. Since sapphire substrates are insulating, a thin layer of gold was sputtered on the BN to avoid charging effects. Once the Au was deposited on the BN on sapphire, the TEM samples were prepared identically for both sources of BN using a FIB lift-out process. The FIB lift-out process was performed in the following way: (i) the sample was coated with a platinum layer deposited in the SEM-FIB system; (ii) trenches were then etched around the area of interest to free it from the substrate, and a nanomanipulator was used to transfer and attach the sample to a copper TEM grid; and finally, (iii) the sample was thinned and cleaned using a low-current, low-energy ion beam.

X-ray photoelectron spectroscopy was conducted using a commercial X-ray photoelectron spectrometer (Kratos Axis Ultra), using a monochromated Al Kα X-ray source ($h\nu$ = 1486.7 eV), electrostatic lens optics, and a multichannel plate and delay line detector coupled to a hemispherical analyzer (180° with a 165 mm mean radius). The photoelectron takeoff angle was normal to the surface of the sample and 45° with respect to the X-ray beam. High-resolution spectra were collected with a pass energy of 20 eV. The pressure in the analysis chamber was typically 2×10^{-9} Torr during data acquisition. Additional XPS spectra were collected using a monochromatic Al K X-ray source and Omicron EA125 hemispherical analyzer. The spectrometer was configured with an acceptance angle of ±8°, a takeoff angle of 45°, and a 15 eV analyzer pass energy, operated in the constant analyzer energy (CAE) mode.

Conflict of Interest: The authors declare no competing financial interest.

Acknowledgment. We appreciate support from the Army Research Office (Grant W911NF1010428) and NRI SWAN. R.M.W. gratefully acknowledges support through an IBM Faculty Award. We thank the National Science Foundation (Grant No. 0618242) for funding the Kratos Axis Ultra XPS used in this work.

Supporting Information Available: Additional results not included in the text. The growth on Cu foils and on Ni at 800 °C. UV–vis measurement and E_g calculation. Additional statistical data from Raman mapping of h-BN on Ni and Raman maps of h-BN on sapphire. Summary of relevant XPS data. This material is available free of charge *via* the Internet at http://pubs.acs.org.

REFERENCES AND NOTES

1. Neto, A. H. C.; Novoselov, K. New Directions in Science and Technology: Two-Dimensional Crystals. *Rep. Prog. Phys.* **2011**, *74*, 082501.
2. Novoselov, K. S.; Geim, A. K.; Morozov, S. V.; Jiang, D.; Zhang, Y.; Dubonos, S. V.; Grigorieva, I. V.; Firsov, A. A. Electric Field Effect in Atomically Thin Carbon Films. *Science* **2004**, *306*, 666–669.
3. Stankovich, S.; Dikin, D. A.; Dommett, G. H. B.; Kohlhaas, K. M.; Zimney, E. J.; Stach, E. A.; Piner, R. D.; Nguyen, S. T.; Ruoff, R. S. Graphene-Based Composite Materials. *Nature* **2006**, *442*, 282–286.
4. Li, X.; Cai, W.; An, J.; Kim, S.; Nah, J.; Yang, D.; Piner, R.; Velamakanni, A.; Jung, I.; Tutuc, E.; *et al.* Large-Area

Synthesis of High-Quality and Uniform Graphene Films on Copper Foils. *Science* **2009**, *324*, 1312–1314.
5. Coleman, J. N.; Lotya, M.; O'Neill, A.; Bergin, S. D.; King, P. J.; Khan, U.; Young, K.; Gaucher, A.; De, S.; Smith, R. J.; *et al.* Two-Dimensional Nanosheets Produced by Liquid Exfoliation of Layered Materials. *Science* **2011**, *331*, 568–571.
6. Mirkarimi, P. B.; McCarty, K. F.; Medlin, D. L. Review of Advances in Cubic Boron Nitride Film Synthesis. *Mater. Sci. Eng., R* **1997**, *21*, 47–100.
7. Paine, R. T.; Narula, C. K. Synthetic Routes to Boron-Nitride. *Chem. Rev.* **1990**, *90*, 73–91.
8. Kubota, Y.; Watanabe, K.; Tsuda, O.; Taniguchi, T. Deep Ultraviolet Light-Emitting Hexagonal Boron Nitride Synthesized at Atmospheric Pressure. *Science* **2007**, *317*, 932–934.
9. Watanabe, K.; Taniguchi, T.; Niiyama, T.; Miya, K.; Taniguchi, M. Far-Ultraviolet Plane-Emission Handheld Device Based on Hexagonal Boron Nitride. *Nat. Photonics* **2009**, *3*, 591–594.
10. Auwarter, W.; Kreutz, T. J.; Greber, T.; Osterwalder, J. XPD and STM Investigation of Hexagonal Boron Nitride on Ni(111). *Surf. Sci.* **1999**, *429*, 229–236.
11. Corso, M.; Auwarter, W.; Muntwiler, M.; Tamai, A.; Greber, T.; Osterwalder, J. Boron Nitride Nanomesh. *Science* **2004**, *303*, 217–220.
12. Nagashima, A.; Tejima, N.; Gamou, Y.; Kawai, T.; Oshima, C. Electronic-Structure of Monolayer Hexagonal Boron-Nitride Physisorbed on Metal-Surfaces. *Phys. Rev. Lett.* **1995**, *75*, 3918–3921.
13. Nagashima, A.; Tejima, N.; Gamou, Y.; Kawai, T.; Oshima, C. Electronic Dispersion-Relations of Monolayer Hexagonal Boron-Nitride Formed on the Ni(111) Surface. *Phys. Rev. B* **1995**, *51*, 4606–4613.
14. Shi, Y.; Hamsen, C.; Jia, X.; Kim, K. K.; Reina, A.; Hofmann, M.; Hsu, A. L.; Zhang, K.; Li, H.; Juang, Z.-Y.; *et al.* Synthesis of Few-Layer Hexagonal Boron Nitride Thin Film by Chemical Vapor Deposition. *Nano Lett.* **2010**, *10*, 4134–4139.
15. Chatterjee, S.; Luo, Z.; Acerce, M.; Yates, D. M.; Johnson, A. T. C.; Sneddon, L. G. Chemical Vapor Deposition of Boron Nitride Nanosheets on Metallic Substrates *via* Decaborane/Ammonia Reactions. *Chem. Mater.* **2011**, *23*, 4414–4416.
16. Ci, L.; Song, L.; Jin, C.; Jariwala, D.; Wu, D.; Li, Y.; Srivastava, A.; Wang, Z. F.; Storr, K.; Balicas, L.; *et al.* Atomic Layers of Hybridized Boron Nitride and Graphene Domains. *Nat. Mater.* **2010**, *9*, 430–435.
17. Kim, K. K.; Hsu, A.; Jia, X.; Kim, S. M.; Shi, Y.; Hofmann, M.; Nezich, D.; Rodriguez-Nieva, J. F.; Dresselhaus, M.; Palacios, T.; *et al.* Synthesis of Monolayer Hexagonal Boron Nitride on Cu Foil Using Chemical Vapor Deposition. *Nano Lett.* **2012**, *12*, 161–166.
18. Lee, K. H.; Shin, H.-J.; Lee, J.; Lee, I.-y.; Kim, G.-H.; Choi, J.-Y.; Kim, S.-W. Large-Scale Synthesis of High-Quality Hexagonal Boron Nitride Nanosheets for Large-Area Graphene Electronics. *Nano Lett.* **2012**, *12*, 714–718.
19. Song, L.; Ci, L.; Lu, H.; Sorokin, P. B.; Jin, C.; Ni, J.; Kvashnin, A. G.; Kvashnin, D. G.; Lou, J.; Yakobson, B. I.; *et al.* Large Scale Growth and Characterization of Atomic Hexagonal Boron Nitride Layers. *Nano Lett.* **2010**, *10*, 3209–3215.
20. Dean, C. R.; Young, A. F.; Meric, I.; Lee, C.; Wang, L.; Sorgenfrei, S.; Watanabe, K.; Taniguchi, T.; Kim, P.; Shepard, K. L.; *et al.* Boron Nitride Substrates for High-Quality Graphene Electronics. *Nat. Nanotechnol.* **2010**, *5*, 722–726.
21. Kim, K.; Choi, J.-Y.; Kim, T.; Cho, S.-H.; Chung, H.-J. A Role for Graphene in Silicon-Based Semiconductor Devices. *Nature* **2011**, *479*, 338–344.
22. Reich, S.; Ferrari, A. C.; Arenal, R.; Loiseau, A.; Bello, I.; Robertson, J. Resonant Raman Scattering in Cubic and Hexagonal Boron Nitride. *Phys. Rev. B* **2005**, *71*, 205201.
23. Baazi, T.; Knystautas, E. J. Hexagonal Boron-Nitride Synthesis by Nitrogen Ion-Implantation of Boron Films. *Thin Solid Films* **1993**, *232*, 185–193.
24. Singh, J. *Electronic and Optoelectronic Properties of Semiconductor Structures*; Cambridge University Press: New York, 2003.
25. Desrosiers, R. M.; Greve, D. W.; Gellman, A. J. Nucleation of Boron Nitride Thin Films on Ni(100). *Surf. Sci.* **1997**, *382*, 35–48.
26. Li, X.; Cai, W.; Colombo, L.; Ruoff, R. S. Evolution of Graphene Growth on Ni and Cu by Carbon Isotope Labeling. *Nano Lett.* **2009**, *9*, 4268–4272.
27. Li, X.; Magnuson, C. W.; Venugopal, A.; An, J.; Suk, J. W.; Han, B.; Borysiak, M.; Cai, W.; Velamakanni, A.; Zhu, Y.; *et al.* Graphene Films with Large Domain Size by a Two-Step Chemical Vapor Deposition Process. *Nano Lett.* **2010**, *10*, 4328–4334.
28. Wriedt, H. A. In *N-Ni (Nitrogen-Nickel), Binary Alloy Phase Diagrams*, 2nd ed.; Massalski T. B., Ed.; Springer: Berlin, 1990; Vol. 3, pp 2693–2694
29. Liao, P. K.; Spear, K. E. In *B-Ni (Boron-Nickel), Binary Alloy Phase Diagrams*, 2nd ed.; Massalky T. B., Ed.; Springer: Berlin, 1990; Vol. 1, p 508–510.
30. Grunze, M.; Golze, M.; Driscoll, R. K.; Dowben, P. A. Ammonia Adsorption and Decomposition on a Ni(110) Surface. *J. Vac. Sci. Technol.* **1981**, *18*, 611–615.
31. Baiker, A.; Maciejewski, M. Formation and Thermal Stability of Copper and Nickel Nitrides. *J. Chem. Soc., Faraday Trans. 1* **1984**, *80*, 2331–2341.
32. Maya, L. Deposition of Crystalline Binary Nitride Films of Tin, Copper and Nickel by Reactive Sputtering. *J. Vac. Sci. Technol., A* **1993**, *11*, 604–608.
33. Gomezaleixandre, C.; Diaz, D.; Orgaz, F.; Albella, J. M. Reaction of Diborane and Ammonia Gas-Mixtures in a Chemical-Vapor-Deposition Hot-Wall Reactor. *J. Phys. Chem.* **1993**, *97*, 11043–11046.
34. Desrosiers, R. M.; Greve, D. W.; Gellman, A. J. Decomposition of B_2H_6 on Ni(100). *J. Vac. Sci. Technol., A* **1997**, *15*, 2181–2189.
35. Liu, Y.; Bhowmick, S.; Yakobson, B. I. BN White Graphene with "Colorful" Edges: The Energies and Morphology. *Nano Lett.* **2011**, *11*, 3113–3116.
36. Auwarter, W.; Suter, H. U.; Sachdev, H.; Greber, T. Synthesis of One Monolayer of Hexagonal Boron Nitride on Ni(111) From B-Trichloroborazine (ClBNH)(3). *Chem. Mater.* **2004**, *16*, 343–345.
37. Auwarter, W.; Muntwiler, M.; Osterwalder, J.; Greber, T. Defect Lines and Two-Domain Structure of Hexagonal Boron Nitride Films on Ni(111). *Surf. Sci.* **2003**, *545*, L735–L740.
38. Bae, C.; Shin, H.; Nielsch, K. Surface Modification and Fabrication of 3D Nanostructures by Atomic Layer Deposition. *MRS Bull.* **2011**, *36*, 887–897.
39. Vickerman, J. C.; Gilmore, I. *Surface Analysis: The Principal Techniques*, 2nd ed.; Wiley: New York, 2009.
40. Jones, A. C.; Hitchman, M. L. *Chemical Vapour Deposition: Precursors, Processes and Applications*; RSC Publishing: London, 2009.